Mechanistic basis of propofol-induced disruption of kinesin processivity

Mandira Dutta[a], Susan P. Gilbert[b,c,1], José N. Onuchic[d,e,f,g,1], and Biman Jana[a,1]

[a]School of Chemical Sciences, Indian Association for the Cultivation of Science, Jadavpur, 700032 Kolkata, India; [b]Department of Biological Sciences, Rensselaer Polytechnic Institute, Troy, NY 12180; [c]Center for Biotechnology and Interdisciplinary Studies, Rensselaer Polytechnic Institute, Troy, NY 12180; [d]Department of Chemistry, Rice University, Houston, TX 77030; [e]Center for Theoretical Biological Physics, Rice University, Houston, TX 77030; [f]Department of Physics and Astronomy, Rice University, Houston, TX 77030; and [g]Department of Biosciences, Rice University, Houston, TX 77030

Contributed by José N. Onuchic, December 22, 2020 (sent for review November 16, 2020; reviewed by Shoji Takada and D. Thirumalai)

Propofol is a widely used general anesthetic to induce and maintain anesthesia, and its effects are thought to occur through impact on the ligand-gated channels including the $GABA_A$ receptor. Propofol also interacts with a large number of proteins including molecular motors and inhibits kinesin processivity, resulting in significant decrease in the run length for conventional kinesin-1 and kinesin-2. However, the molecular mechanism by which propofol achieves this outcome is not known. The structural transition in the kinesin neck-linker region is crucial for its processivity. In this study, we analyzed the effect of propofol and its fluorine derivative (fropofol) on the transition in the neck-linker region of kinesin. Propofol binds at two crucial surfaces in the leading head: one at the microtubule-binding interface and the other in the neck-linker region. We observed in both the cases the order–disorder transition of the neck-linker was disrupted and kinesin lost its signal for forward movement. In contrast, there was not an effect on the neck-linker transition with propofol binding at the trailing head. Free-energy calculations show that propofol at the microtubule-binding surface significantly reduces the microtubule-binding affinity of the kinesin head. While propofol makes pi–pi stacking and H-bond interactions with the propofol binding cavity, fropofol is unable to make a suitable interaction at this binding surface. Therefore, the binding affinity of fropofol is much lower compared to propofol. Hence, this study provides a mechanism by which propofol disrupts kinesin processivity and identifies transitions in the ATPase stepping cycle likely affected.

kinesin | propofol | fropofol | anesthetic mechanism | neuron

Propofol (2,6-diisopropylphenol) is a widely used intravenous general anesthetic to induce and maintain anesthesia (1–4). It is a small hydrophobic molecule, and upon binding propofol can alter the activities of ligand- and voltage-gated channels including the $GABA_A$ receptor and others (5–11). It is the change in their activities that is believed to lead to the desirable clinical effects including unconsciousness, analgesia, amnesia, and immobility. However, through the use of photoactive derivatives of propofol many other target proteins have been discovered, leading to an emerging hypothesis that the state of anesthesia is a result of a network of target proteins including the intracellular transport kinesins (4, 11).

Conventional kinesin-1 (KIF5) and two heterodimeric kinesin-2s (KIF3AC and KIF3AB) were shown to be inhibited by the anesthetics propofol, ketamine, and etomidate at clinically relevant concentrations with a similar inhibition profile (12), suggesting that kinesins may contribute to the anesthetic effects on memory and consciousness. There are 45 human kinesin genes, 38 of which are expressed in brain, with 15 to 20 kinesins thought to mediate long-range, microtubule (MT)-based vesicle transport in neurons (reviewed in refs. 13–16). The transport kinesins are dimeric with their catalytic motor domains dimerized through a coiled-coil stalk with globular carboxyl-terminal domains that interact with specific adaptors for cargo binding. From each motor domain there is short ∼14-residue peptide, termed the neck linker (NL), that connects each of the kinesin heads to the common stalk (17–19).

The movement of these kinesins is precise with each adenosine 5′-triphosphate (ATP) turnover coupled to an 8-nm step, the distance between adjacent αβ-tubulin dimers along the MT lattice, and kinesins as single molecules can complete 100 steps or more in an asymmetric hand-over-hand manner (20–23). This behavior has been referred to as "processive movement" with the distance a kinesin travels along the MT before detachment defined as its run length. To maintain processive stepping, the ATPase cycle of each motor domain must be coordinated such that they remain out of phase with each other. If both motor heads were to reach the adenosine 5′-diphosphate (ADP)-bound weak binding state to the MT the kinesin motor with cargo completely detaches from the MT, ending the processive run.

In single-molecule motility studies, propofol reduced the overall run length for kinesin-1 and kinesin-2 KIF3AB and KIF3AC by 40 to 60% with half maximal effective concentration <100 nM propofol without an effect on the velocity of movement (12). These results indicated that propofol was not binding to the ATP-binding site or to allosteric sites that modulate MT-activated ATP turnover, suggesting that a transient propofol allosteric site forms when the motor head binds to the MT during kinesin stepping. Moreover, when the single-molecule experiments were repeated with fropofol, a propofol analog in which the 1-hydroxyl group was substituted with fluoride, there was no effect on kinesin motility, suggesting that the propofol hydroxyl group was required to form the allosteric site during the processive run (12). Note that fropofol

Significance

Kinesins are the major transporters of cargos toward the cell periphery, and their dysfunction leads to a range of human pathologies. Anesthetics used in surgery can shorten the distance that kinesins travel. We show that propofol binds at two crucial sites on the motor domain of the leading head, one at the microtubule interface and the other at the neck-linker region. In both cases, propofol disrupts the order–disorder transition of the neck linkers, resulting in loss of the signal for kinesin to step forward. In contrast, there was not an effect by propofol binding at the trailing head. These results provide a mechanism by which propofol disrupts kinesin stepping, which may diminish their ability to transport critical cargos.

Author contributions: M.D., S.P.G., J.N.O., and B.J. designed research, performed research, analyzed data, and wrote the paper.

Reviewers: S.T., Kyoto University; and D.T., University of Texas at Austin.

The authors declare no competing interest.

[1]To whom correspondence may be addressed. Email: sgilbert@rpi.edu, jonuchic@rice.edu, or pcbj@iacs.res.in.

This article contains supporting information online at https://www.pnas.org/lookup/suppl/doi:10.1073/pnas.2023659118/-/DCSupplemental.

Published January 25, 2021.

cannot induce anesthesia or the sedative properties associated with propofol, yet fropofol can cause similar adverse cardiovascular effects as observed for propofol (24).

Subsequent studies identified the kinesin allosteric sites using a photoactive derivative of propofol in combination with semi-quantitative radiolabeling and microsequencing assays (25). The results were consistent for the three kinesins, where there was little labeling of free kinesin in solution or MTs but labeling was predominantly localized to the motor domain of the MT•kinesin complex in the presence of the nonhydrolyzable ATP analog, AMPPMP. Woll et al. identified the photolabeled residues of kinesin-1 and kinesin-2 motor domains (25) and mapped these residues onto the X-ray crystal structures of the tubulin-kinesin motor domain without nucleotide, the apo state (Protein Data Bank [PDB] ID code 4LNU; ref. 26) and the tubulin-kinesin motor domain with ADP aluminum fluoride that is considered representative of the ATP state (PDB ID code 4HNA; ref. 27). The results suggested that the propofol binding site was specific for these three kinesins and that the binding pocket identified within the AMPPNP-bound MT•kinesin complex better represents the high-affinity and/or propofol-specific site (25). What was most compelling was that the propofol binding site localized near the NL, which is a critical mechanical element to maintain head–head communication to coordinate the two heads as they step processively (25).

These experimental observations can now be explained completely by our theoretical framework that shows that processivity is directly connected to the synergy between the ability of the motor to bind to the MT and the order/disorder transition of the NL which controls the structure and binding ability of the kinesin pocket to the nucleotides. Disruption in any of these two effects may disrupt motor processivity and directionality. A recent review article provides a detailed discussion of the underlying physical mechanisms governing the function of kinesin and other motor proteins (28).

Results and Discussion

Conventional kinesins are able to carry out ~100 steps before detachment from the MT (29). Various studies regarding the

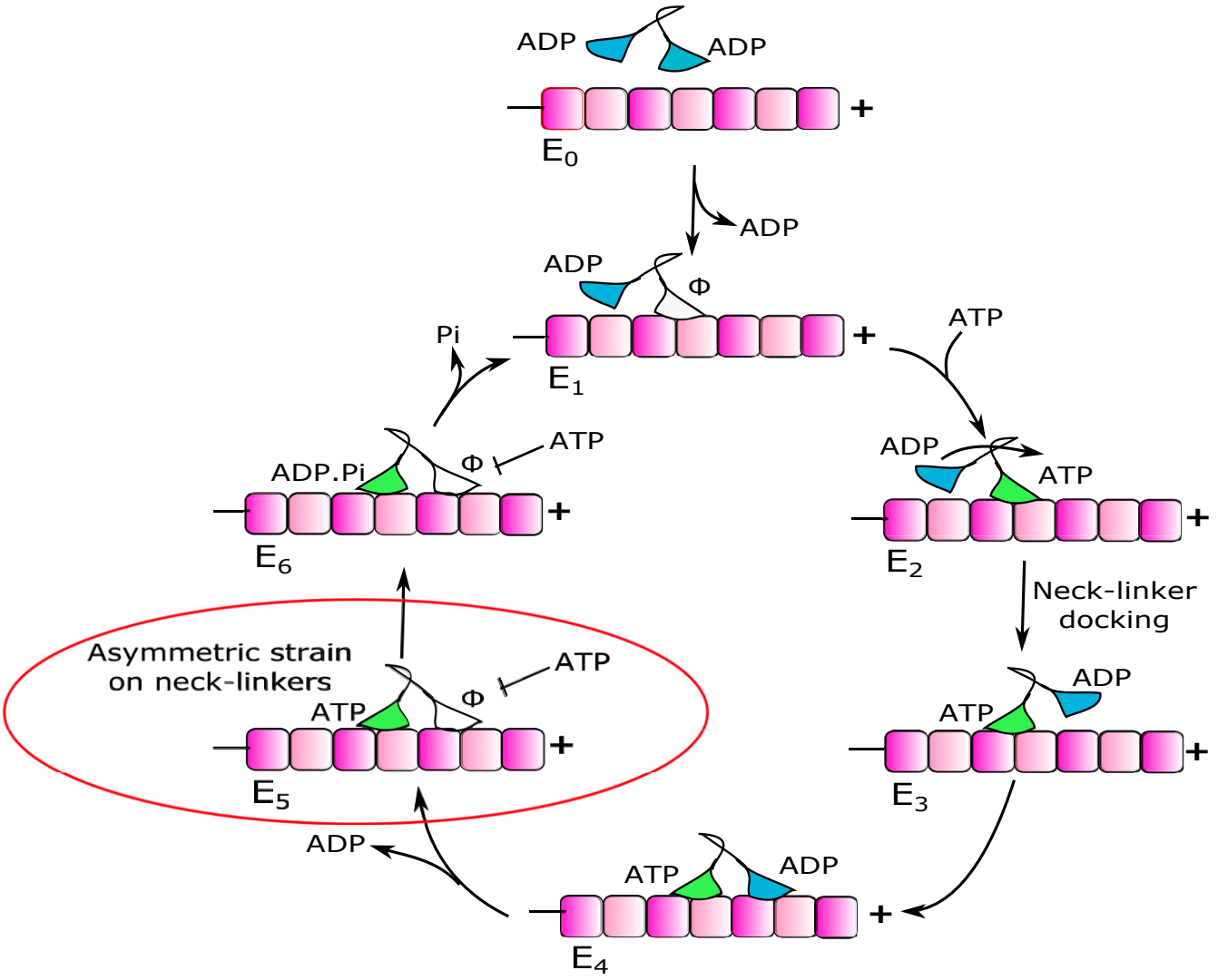

Fig. 1. Mechanochemical cycle of kinesin stepping. (E_0) Dimeric kinesin in solution. (E_1–E_3) E1 represents the ATP-waiting state with the leading L head bound tightly to the MT and the trailing T head detached from the MT with ADP bound at its active site. The L head binds ATP (E2), which leads to the diffusive movement of ADP-bound T head toward the next binding site on MT (E3). (E_4–E_6) Two-head-bound state of kinesin to the MT. The release of ADP from the L head generates asymmetric strain on the NLs of L and T heads (E_5 state, red circle). Strain on the NL of the L head is much higher than that of the T head. ATP hydrolysis and Pi release results in an ADP weakly bound state at the T head, intermolecular strain is reduced, and the L head becomes tightly bound to the MT, reforming the ATP-waiting state (E_1).

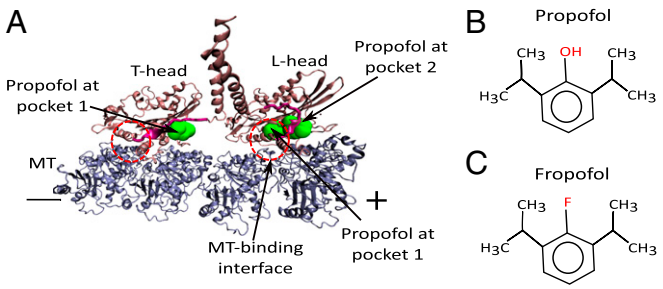

Fig. 2. Propofol binding pocket in the L and T heads of kinesin. (*A*) The L head has two propofol binding sites. Pocket-1 is close to the MT binding surface and pocket-2 is far from the MT interface. The T head has only one propofol binding site, pocket-1 which is far from the MT-binding interfaces. The circles with red dotted lines show MT-binding interfaces. (*B*) Propofol, 2,6-diisopropylphenol. (*C*) Fropofol, 2-fluoro-1,3-diisopropylbenzene.

structural and dynamical aspects of kinesin suggest that for this kind of processive movement at least one head remains strongly attached with the MT during the mechanochemical cycle to prevent premature detachment (30). To maintain such coordination, two motor heads need a mechanism to communicate between their nucleotide and structural states. It has been proposed that this communication is mediated through the internal load generated in a configuration when both the leading (L) and trailing (T) heads are tightly bound to the MT (31). A simplified version of the mechanochemical cycle is shown in Fig. 1. It has been suggested that in this cycle, the two-head-bound E5 state (shown in a red circle in Fig. 1) is important for the processive movement of kinesin (32, 33). In this state, the binding of ATP at the L head is inhibited to ensure that the two heads remain out of phase with each other rather than entering an ADP weak binding state with the MT. The NL remains in either the docked (ordered) or undocked (disordered) state dependent upon the nucleotide state at the active site. Previous studies have revealed that in the E5 intermediate the NL of the T head is docked, but in the L head it is undocked due to the internal strain (34, 35). In such a situation, the nucleotide binding pocket of the L head adopts a disordered configuration that is not suitable for ATP binding. Upon detachment of the T head from MT, the internal strain is released. Therefore, the L head can now bind to ATP, leading to the NL transitions from the undocked to the docked state (34, 35). These transitions allow for the diffusive search of the T head biased toward the MT plus-end to its next binding site 16 nm away. Thus, different states of the NLs for the two heads of kinesin in the E5 state are crucial for the coordination of the two heads of kinesin to step processivity for long-distance movement (34–36). Any perturbations that can negatively affect this coordination such as mutations or small-molecule binding in the motor domain can hamper kinesin's processivity (12, 25, 37, 38).

Recently, Bensel et al. (12) and Woll et al. (25) revealed that the widely used general anesthetic propofol significantly decreases the average run length of kinesin-1 and kinesin-2 in single-molecule assays, although the velocity of movement remained unchanged. In the work presented here, we investigated the mechanisms by which propofol affects kinesin's processivity when it is bound to the L head or T head in the two-head-bound condition (Fig. 1, E5 intermediate). In this state, the L head is nucleotide-free and the T head is bound to ATP, which results in asymmetric strain on the NLs. This study aims to evaluate the consequences of propofol binding on the order–disorder states of the NLs of the E5 intermediate.

For a comprehensive understanding of the mechanism, we have used the following procedures. First, a coarse-grained structure-based model (SBM) was built to investigate the effect of propofol binding on the processivity of kinesin, and second an all-atom physical force field including explicit solvent simulation was used to determine how propofol interacts with the kinesin head. Previously, these methodologies were used successfully to explore the mechanisms of different motor proteins (34, 38–49). For these studies, two kinesin X-ray crystal structures were considered. PDB ID code 4LNU (26) provided the tubulin-bound apo-kinesin state representing the L head of the E5 intermediate, while PDB ID code 4HNA (27) provided the tubulin-bound ATP state of the T head. To explore the possible binding pockets

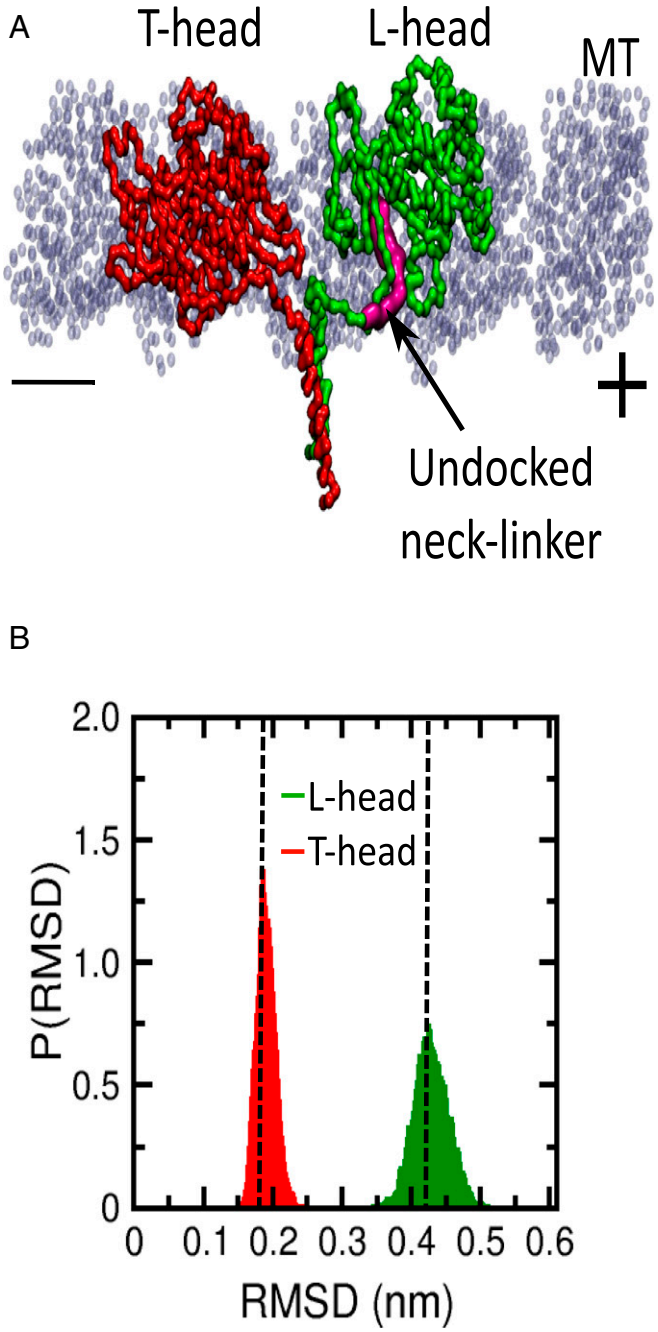

Fig. 3. The two-head-bound state (E_5) to the MT shows asymmetry between L (green) and T (red) heads. (*A*) The NL of the L head remains undocked due to the strain. (*B*) The rmsd of the L head is higher (peak at 0.42 nm) than the T head (peak at 0.18 nm), which indicates a larger deviation from the initial native state. Rmsd was calculated with respect to the crystal structure (PDB ID code 3KIN) of the initial solution state of kinesin in the absence of the MT.

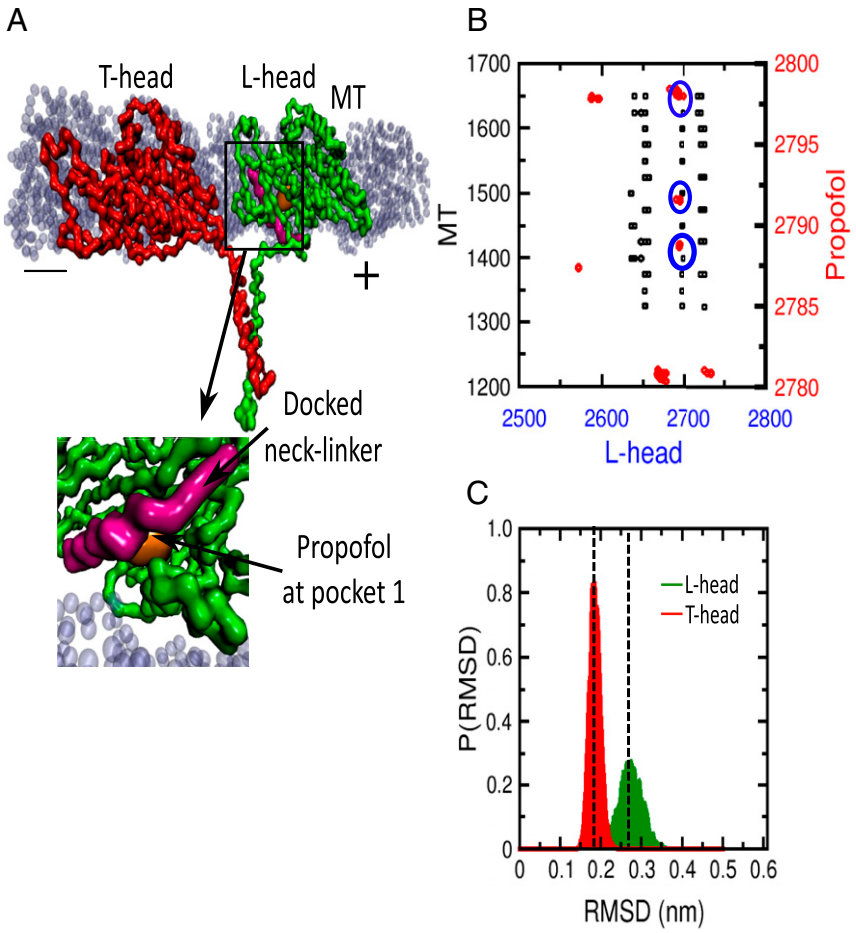

Fig. 4. Consequences of propofol binding at pocket-1 of the L head at the MT–kinesin interface. (*A*) A snapshot was taken from the coarse-grained molecular dynamics simulation trajectory. Pocket-1 is in close vicinity of the MT-binding surface. The NL of the L head shows a docked conformation. (*B*) There are common contacts (blue circles) between the L head and MT and propofol. (*C*) Peak values of the rmsd distributions for the L head and T head are 0.26 nm and 0.18 nm, which are close to each other.

of propofol in these two states of kinesin, the docking simulations were performed using the AutoDockVina (ADV) software (50). The propofol binding pockets with the highest scores are shown in *SI Appendix*, Fig. S1 (see *SI Appendix*, Tables S1 and S2 for the ADV scores of 4LNU and 4HNA, respectively). In the nucleotide-free L head, two binding pockets with very close highest score values were observed: Pocket-1 is close to the MT binding interface while pocket-2 is in a distant position from the MT surface but closer to the NL region (*SI Appendix*, Fig. S1*B*). In the T head, one pocket (pocket-1) with a high score value was obtained. The T-head pocket-1 is found to be far away from both the MT-binding interface and the NL (*SI Appendix*, Fig. S1*A*). We superimposed the apo-head (4LNU) with the L head and ATP-bound head (4HNA) with the T head of the two-head-bound E5 intermediate. Fig. 2 shows the binding pockets of L and T heads in the E5 intermediate.

To explore the effect of propofol binding on kinesin during the mechanochemical cycle, we have performed molecular dynamics simulations of kinesin–MT complexes (with and without propofol) and kinesin heads (with propofol or fropofol) in solution using the coarse-grained and the detailed force fields described above. Using the methodology developed earlier by our group (51–54), we first prepared the coarse-grained SBM of the kinesin dimer where both heads are bound to the MT to mimic the E5 state. Subsequently, we have performed stochastic dynamics simulation of the same state to uncover the structural ensemble of the two-head-bound state. It is important to mention that the dimeric kinesin structure in the absence of the MT (E_0) is symmetric where both the heads have negligible structural distortions, that is, no strain is present (55). First, we assessed the configurations of the two NLs related to the L and T heads in the E5 state of dimeric kinesin in the absence of propofol (Fig. 3). We observed that while the NL of the T head remains in its initial docked state as expected, the configuration of the NL of the L head changes significantly and becomes undocked from the motor domain (Fig. 3*A*). From the rmsd (relative to the crystal structure) distribution plot, we observed that the L head shows its peak value around 0.42 nm and T head at 0.18 nm (Fig. 3*B*). Consistent with our previous studies, this observation indicates an asymmetry between the two heads in the MT-bound condition. Here the undocked NL of the L head creates strain that ultimately perturbs the structural state, particularly of the nucleotide binding pocket of the L head. Previously, we showed that this structural asymmetry between L and T heads in the E5 intermediate is very important for the motility of kinesin (34, 38). Please note that such asymmetry is also related to the order to disorder (docked to undocked) transition of the NL of the L head.

As discussed earlier, the leading head has two propofol binding pockets; one is close to the MT-binding interface and the other is in the NL region. Hence, to investigate the mechanisms of how propofol affects the processivity of kinesin when bound to the L head, we have divided our results into three parts. First (Effect 1), we have presented the consequences of propofol binding at the MT–head interface. Next (Effect 2), we examined the results when propofol is absent but instead the MT–head interaction is

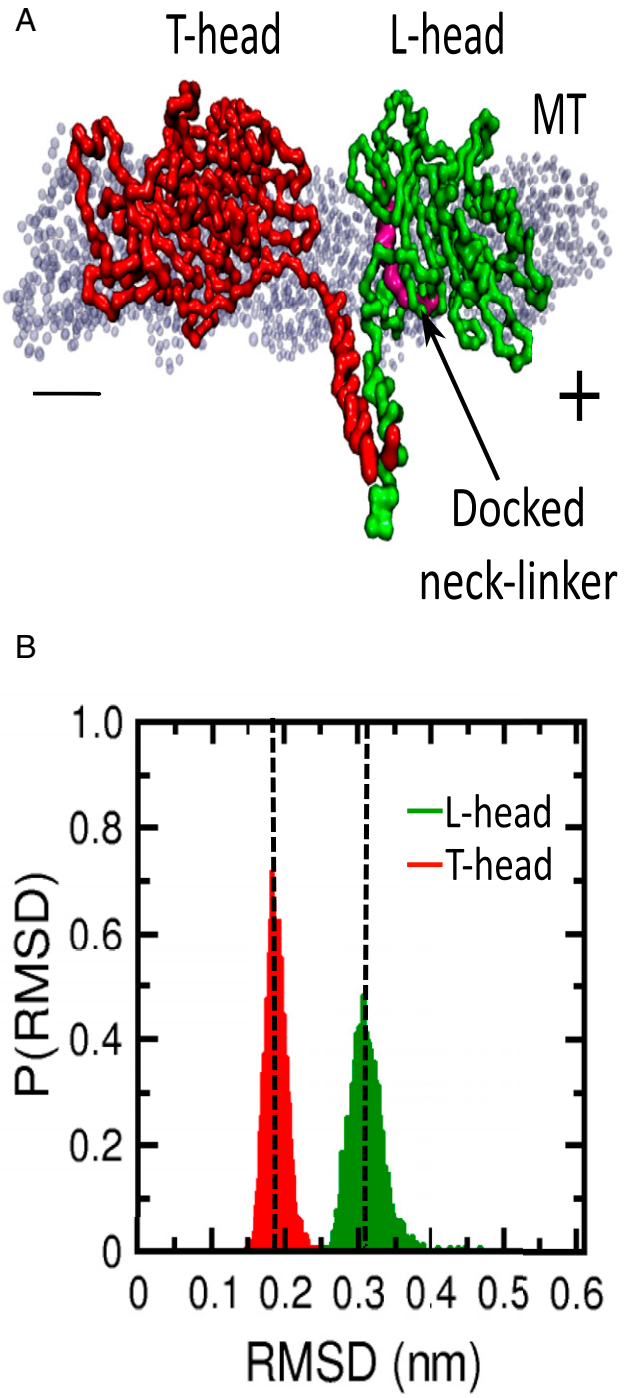

Fig. 5. Disruption of the asymmetry between the L and T heads after mutating the common contact pairs between the MT and kinesin-head interface when propofol is absent. (*A*) The L head shows a docked NL. (*B*) The rmsd of the L head decreases significantly.

destabilized to mimic the implicit binding of propofol, a simpler implicit version of Effect 1. Finally, we investigated the effect of propofol binding at the NL region of the L head (Effect 3). The propofol binding at the T head of kinesin is discussed separately. All our studies assume that propofol binding and unbinding is sufficiently fast and that the occupation of these binding sites by propofol is sufficiently high to make these effects significant. This appears to be true for the experiments analyzed here, but clearly these results will depend on propofol concentration.

Propofol Binding at the L Head.

Effect 1. In this section, we focused on pocket-1 of the L head which is located at the kinesin–MT interface region (Fig. 4*A*). We generated a contact map of the MT–head interface including propofol using the SMOG@ctbp server (51). We found that propofol and the MT interact indirectly through common residues of the L head because propofol binds to the MT–head interface region (Fig. 4*B*). Blue circles in Fig. 4*B* show the regions of the L head through which the MT and propofol interact. To further explore this situation, we developed a coarse-grained SBM of a dimeric kinesin bound to MT (E5 state) where propofol is bound to the MT binding interface of the L head. From Fig. 4*C*, it is evident that the rmsd values of the L and T heads are now 0.18 nm and 0.26 nm, respectively. This result indicates significant reduction of the asymmetric nature between the two heads when compared to the results obtained in the absence of propofol (Fig. 3*B*). Most importantly, the NL of the L head shows a docked conformation (Fig. 4*A*). Therefore, propofol binding to the MT binding interface region of the L head affects the order–disorder transition of the NL and thereby dissipates the structural asymmetry needed for functionality between the two heads significantly.

Effect 2. We mentioned earlier that there are few common residues of the L head which can interact with both the MT and propofol (Fig. 4*B*). We hypothesized that upon propofol binding these common contacts between the MT and L head will be destabilized. To this end, we have removed these interactions between the MT and L head that are common with propofol to implicitly include the propofol effect. Instead, we provide a repulsive potential to these contact pairs of the L head and MT in our SB Hamiltonian in its two-head-bound state (E5 intermediate). Please note that propofol is not present in this model explicitly, but contact modifications ensure its implicit presence in the pocket-1. We observed that the rmsd (Fig. 5*B*) of the L head decreases significantly (0.30 nm) compared to Fig. 3*B*, and the NL of the L head is in a docked conformation (Fig. 5 *A* and *B*). Thus, we propose that propofol binding to the L head at the kinesin–MT interface compromises the binding strength of the L head to the MT. As a result, there is significant strain reduction in the NL of the L head in the E5 state. In such a situation, the conformation of the NL of the L head becomes docked and ultimately reduces the structural asymmetry between the two heads.

Effect 3. Next, we focused on pocket-2 of the L head. Although this binding pocket is far from the MT–kinesin interface, it is very close to the NL region of the L head. We observed from the contact map analysis that propofol directly interacts with the NL region of the L head (Fig. 6*B*). Consequently, we built the SBM of the two-head-bound dimeric kinesin in its E5 state considering propofol at binding pocket-2. Rmsd calculations in Fig. 6*C* show that the L head has an rmsd value of ∼0.29 nm, which is similar for the T head at ∼0.18 nm. These results signify that the asymmetry of the two heads has disappeared considerably, and the NL of the L head is found to be in a docked conformation (Fig. 6*A*).

These results suggest that for both binding sites propofol in the L head reduces the structural asymmetry between L and T heads in its two-head-bound E5 state. As a consequence, it significantly disturbs the order–disorder transition of the NL of the L head. Our previous studies suggest that any perturbations in the MT–head interface and/or in the coiled-coil dimerization region of dimeric kinesin in its E5 state can potentially disrupt structural asymmetry between the two heads in the MT bound condition and thereby affect the processivity of the kinesin (38). Here, propofol binding in pocket-1 can affect the MT-binding strength and therefore can modulate the order–disorder transition of NL. On the other hand, direct interaction of propofol with the NL region can also affect the order–disorder transition of the NL of the L head.

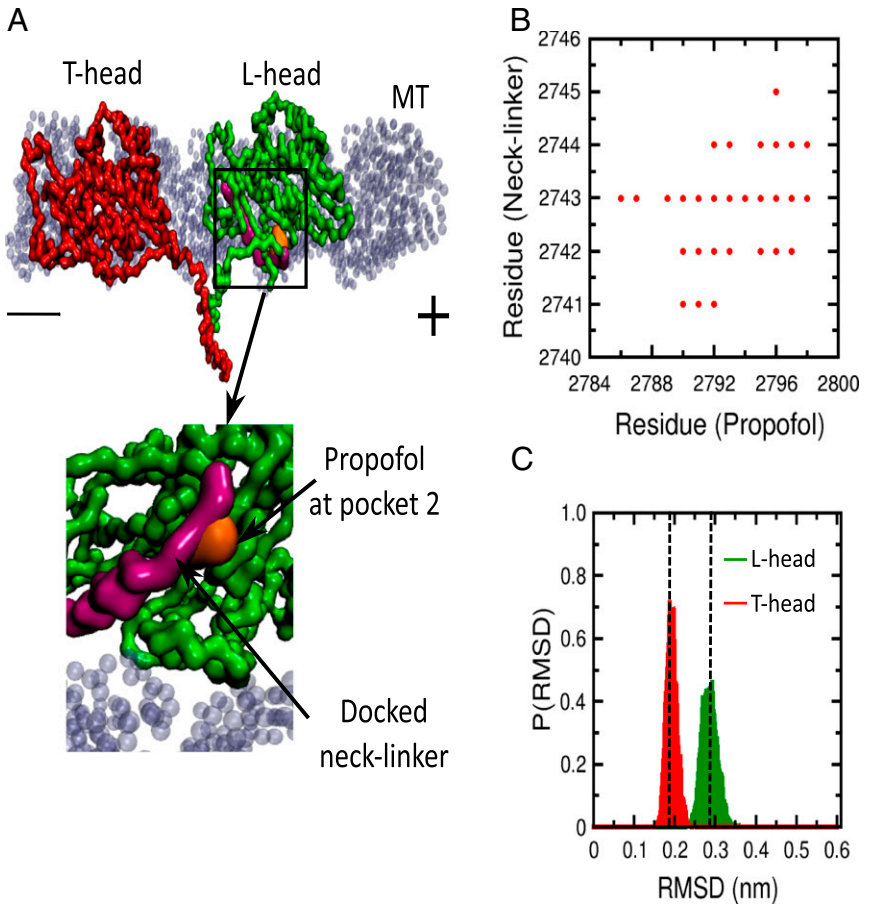

Fig. 6. Consequences of propofol binding at pocket-2. (*A*) A snapshot was taken from the coarse-grained molecular dynamics simulation trajectory. Pocket-2 is very close to the NL coil of the L head. The NL of the L head shows a docked conformation. (*B*) Contact map shows propofol directly interacts with the NL. (*C*) The rmsd of the L head (peak value 0.29 nm) decreases significantly, which signifies break down of asymmetry between the two heads.

Effect of Propofol Binding on the T Head. Because propofol binding at the T head may also affect the run length of kinesin by inhibiting its order–disorder transition, we tested this hypothesis directly. We built the SBM for the two-head-bound kinesin in its E5 state with propofol in the T head. The propofol binding surface in the T head is away from both the MT-binding surface and from the NL region (Fig. 7*A*). Fig. 7*B* suggests that there are no common contacts or direct contacts of propofol with these two important regions (MT–head and NL) as the MT and NL regions range from residue numbers 1 to 2070 and 2439 to 2447, respectively, in the two-head-bound structure of our model (see *Materials and Methods* for details). Interestingly, we found that the rmsd of the L head is ∼0.41 nm and that of T head is ∼0.18 nm (Fig. 7*C*). These values are similar to those observed in the case of the kinesin dimer bound to MT in its E5 state without propofol. Therefore, propofol binding to the T head retains the asymmetry of the structural ensembles between two heads. Most importantly, the NL of the L head remains undocked as in the case of propofol-free kinesin in the E5 state (Fig. 7*A*). Therefore, propofol binding in the T head has no direct effects on the processivity of kinesin.

Change in MT-Binding Affinity upon Propofol Binding at Pocket-1 of the L Head. To quantify the effect of propofol binding at pocket-1 on the MT–head interactions of kinesin we went beyond the coarse-grained models and calculated its binding free energy by estimating the potential of mean force (PMF) of the MT and kinesin head using all-atom explicit solvent simulations and the umbrella sampling method (56). Fig. 8 shows that the binding free energy at the minimum is destabilized by ∼20 kJ/mol when propofol is bound compared to the propofol-free state. This result suggests that propofol binding to the L head in the E5 state weakens its MT binding affinity that leads to loss of the asymmetric nature of the structural states between the two NLs of E5 state.

Local Interactions of Propofol and Fropofol within the Kinesin Motor Domain. To investigate the local molecular level picture, we have performed all-atom molecular dynamics simulations of the kinesin head in explicit solvent. In these simulations, propofol makes pi–pi stacking and H-bond interactions with the kinesin head at the MT-binding surface (Fig. 9*B*). Fig. 9*D* shows that the 1-hydroxyl group of propofol makes an H-bond with the backbone –CO group of 258Leu. The distribution of O–O distances shows a peak at 0.35 nm (*SI Appendix*, Fig. S2*A*). Additionally, the phenyl ring of propofol forms pi–pi stacking interactions with 318Phe of the kinesin head (Fig. 9*D*). The distribution of pi–pi stacking distances between phenyl ring of propofol and phenyl ring of 318Phe shows its peak at 0.45 nm (*SI Appendix*, Fig. S2*A*). A representative snapshot depicting H-bond and pi–pi stacking interactions of propofol with the kinesin head is shown in Fig. 9*D*.

Bensel et al. reported that fropofol, which is a fluorine derivative of propofol in which the 1-hydroxyl of propofol is substituted with fluoride, does not decrease the run length of kinesin as observed for propofol (12). There are two possible interpretations of these results. Either fropofol, which lacks the 1-hydroxyl group, cannot bind to kinesin with high enough affinity to decrease its run length observed with propofol or, alternatively, fropofol is bound

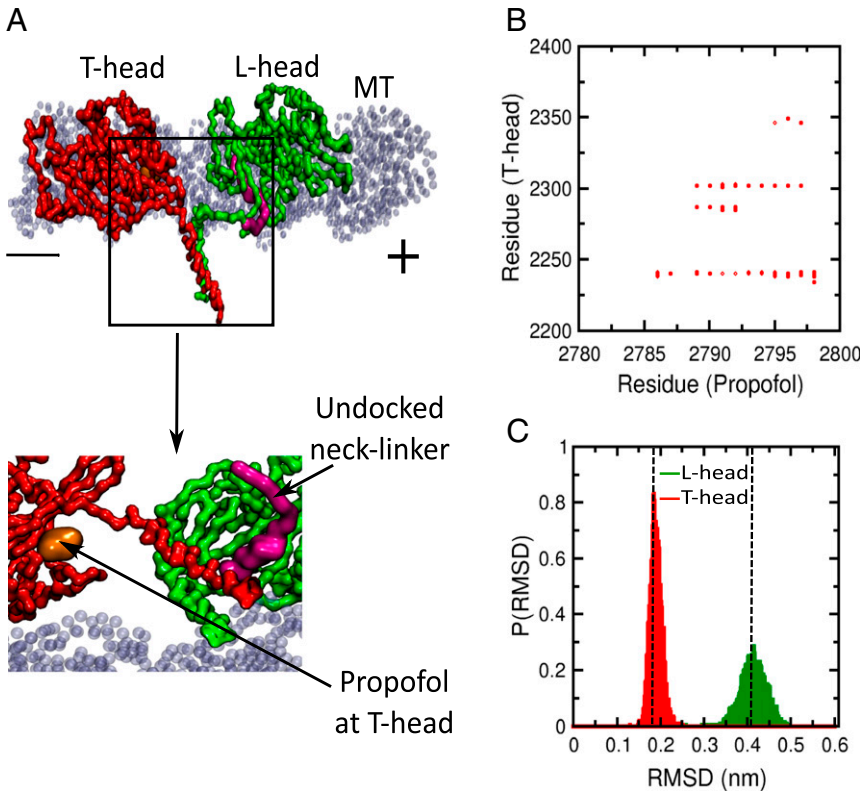

Fig. 7. Effect of propofol binding at the T head. (*A*) A snapshot was taken from the coarse-grained molecular dynamics simulation trajectory. The propofol binding pocket is far from both the NL and MT-head interface. The NL remains undocked in the L head. (*B*) Propofol does not show any direct or common contact with NL or MT-binding surfaces. The MT–kinesin interface and NL domain ranges from 1 to 2070 and 2739 to 2747 residue numbers, respectively, in our model. (*C*) The L head rmsd is much higher (0.41 nm) than the T head (0.18 nm), which indicates persistence of asymmetry between two heads.

but cannot disrupt the order–disorder interactions between the kinesin heads that lead to kinesin detachment from the MT prematurely. To explore these two possibilities, we checked the binding affinity of fropofol at pocket-1 of the L head of kinesin at the MT binding interface region (Fig. 2) by calculating binding free energy. We used the umbrella sampling technique (56) to assess the distance between propofol or fropofol and the binding pocket as an order parameter. From the PMF plots, it is evident that the binding free energy for propofol is at a minimum more stable by ∼60 kJ/mol compared to fropofol at pocket-1 of the L head (Fig. 9*A*). The thermodynamic picture suggests that fropofol cannot properly interact with the binding site. Further investigations demonstrated that fropofol is unable to make the H-bond interaction with the binding pocket because of the absence of the 1-hydroxyl group of propofol. Additionally, the calculated distances between the two benzene rings of fropofol and 318Phe show higher fluctuations than observed for propofol (Fig. 9*C*). The distance distribution plot is broad for fropofol with a peak around 0.57 nm and a tail toward the larger distances (*SI Appendix*, Fig. S2*B*), which indicates the absence of suitable pi–pi stacking interactions. In a previous study, Qiu et al. calculated the binding energy of propofol and fropofol in three different proteins (57). In their study, they found that the differences in binding energies between propofol and fropofol for some of the proteins are in the range of values similar to those obtained in our calculations. Our study also showed that fropofol failed to show any effect on the kinesin's run length as a consequence of the lack of proper interactions at the propofol binding site. A representative snapshot of fropofol bound to the kinesin head is shown in Fig. 9*E*. It is evident that the phenyl ring of fropofol is shifted toward a configuration in which pi–pi interaction with 318Phe is unfavorable.

Discussion

Experimental evidence suggests that propofol, a widely used anesthetic agent, inhibits kinesin run length and processivity (12, 25). However, we still lack the molecular-level picture of the interactions and their consequences on the kinesin motor protein. In this study, we used all-atom explicit solvent simulations and coarse-gained SBM simulations, along with different free-energy calculation methods, for a comprehensive understanding of the mechanisms governing propofol disruption. A large number of previous studies suggested the importance of order–disorder transition of NL for the forward movement of kinesin (31–35). Here we investigated the effect of propofol binding and its impact on the order–disorder transition of NL (Fig. 10). Propofol binds at two crucial surfaces, the MT-binding interface and the NL region in the L head. We observed that in the two-head-bound condition (E5 intermediate), propofol at both binding surfaces inhibits the order–disorder transition of the NL of kinesin and thereby disturbs the asymmetry nature between two heads. Therefore, kinesin lacks the signal for the processive forward movement. Propofol in the T head has a negligible effect because the binding pocket is in a distant position from the MT-binding and/or NL regions. Therefore, the T-head effect can be ignored. Free-energy calculations show that the MT-binding affinity decreases in the presence of propofol at the MT-binding surface. We determined that propofol makes a pi–pi stacking and H-bond interactions with binding pocket-1 in the L head. Fropofol, a propofol fluorine derivative, lacks a suitable interaction with the binding pocket. As a result, fropofol has a low binding affinity compared to propofol. Our conclusions are well supported by the experimental work of Bensel et al. (12) and Woll et al. (25). They observed that propofol disrupts kinesin motility by reducing the run length significantly

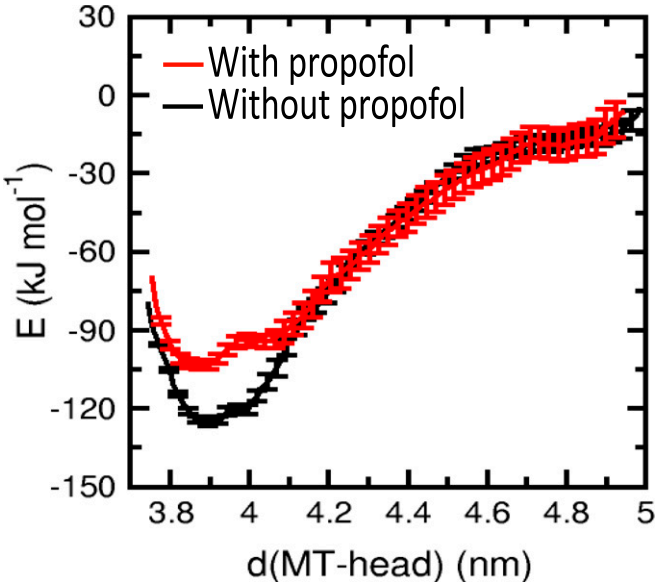

Fig. 8. PMF of the MT-binding affinity of the kinesin head in presence (red) and absence (black) of propofol. Propofol destabilizes the MT-binding affinity of the kinesin head relative to the state in the absence of propofol. Here d(MT-head) indicates COM distance of head domain from MT where d represents distance.

whereas fropofol showed no significant effect on run length and was similar to the results obtained in the absence of propofol. Therefore, this study is important in that it provides a probable mechanism by which propofol, and possibly other anesthetics, disrupt kinesin long-distance transport. Most important, the agreement between theory and experiments provides additional support to our proposed theoretical model of the mechanism governing kinesin processivity.

Materials and Methods

System Preparation. The two-head-bound crystal structure of kinesin has not been reported yet. Therefore, following our previous studies (38, 44), we manually built a model system where two heads bound with the MT using the crystal structures available in the PDB. In the dimeric crystal structure of kinesin [PDB ID code 3KIN (55)], each monomer folds into its native state in absence of MT. We used the crystal structure of single head bound to the MT (PDB ID code 4HNA) (27) and superimposed this structure to dimeric kinesin. Next, we broke a few contacts related to NL and NL binding sites in the motor domain head. Additionally, we modified the structure of 3KIN around the NL region of the L head to generate a two-head-bound state of kinesin. Now, the interactions of each kinesin head with its MT binding site provides a minimum-energy structure which is different from the native dimeric crystal structure without the MT. The initial structure was relaxed, and an ensemble of equilibrated dimeric kinesin on the MT was obtained. To dock propofol in the kinesin head, we used ADV (50), which is a well-tested optimized method to perform docking experiments. The input structure files were prepared using AutoDock Tools (58) by adding hydrogens and Kollman charges and by merging the nonpolar hydrogens. In a previous experimental study by Woll et al. (25) they mapped the preferred binding sites of propofol in the kinesin head in the kinesin–MT complex using a photoactive derivative of propofol, meta-azipropofol (AziPm), followed by mass spectrometry microsequencing. Based on these studies, we validated our docking simulations.

SBM of Kinesin. To access the alteration of order–disorder transition of NLs in different propofol bound states we developed the SBM of kinesin. The SBM is built based on the energy landscape theory of protein folding (54, 59–61). The SBM force field stabilizes the interactions present in the native configurations and ignores the frustration due to nonnative interactions. All nonnative interactions are considered repulsive and therefore the landscape is perfectly funneled (53, 62, 63). In this study, the SBM models were built based on the MT-bound dimeric structure of kinesin for both cases, in presence and absence of propofol, using the SMOG2@ctbp server (51). The Cα coarse-grained model was developed utilizing a single bead at the Cα position of each amino acid residue of the protein and at each heavy atom of propofol. The ranges of the residue number for different regions of dimeric kinesin bound to the MT and a single propofol at the kinesin head are as follows: 1 to 2784 for MT, 2071 to 2432 for T head (2385 to 2393 for the NL), 2433 to 2784 for L head (2739 to 2747 for the NL), and 2785 to 2798 for propofol. To account for the interactions between propofol and kinesin head/MT, an attractive contact-like potential was added for the pair of residues between Cα atom of kinesin head/MT and heavy atom of propofol when the distance between them is within 10 Å in the docked structure.

The Hamiltonian is

$$H_{SBM}\{(\vec{r}_i)\} = H_B + H_{NB}.$$

Here H_B and H_{NB} represent the local bonded and nonbonded components, respectively.

$$H_B = \sum_{i=1}^{N-1} \frac{K_r}{2}\left(r_{i,i+1} - r^0_{i,i+1}\right)^2 + \sum_{i=1}^{N-2} \frac{K_\theta}{2}\left(\theta_i - \theta^0_i\right)^2 + \sum_{i=1}^{N-3} \sum_{n=1,3} K^{(n)}_\phi\left(1 - \cos\left[n\left(\phi_i - \phi^0_i\right)\right]\right).$$

The first term $r_{i,i+1}$ is the distance between residues i and i+1 and is constrained harmonically by a spring constant K_r = 200 (kJ·mol^{-1}·Å^{-2}) with respect to the native distance $r^0_{i,i+1}$. In the second term, θ_i represents the angle between residues of i, i+1, and i+2 and it is constrained with respect to native value, θ^0_i, by a harmonic spring constant K_θ with value 40 (kJ·mol^{-1}·rad^{-2}). The third term represents the dihedral angle potential which describes the rotation of the backbone involving successive residues from i to i+3 with $K^{(1)}_\phi = 2K^{(3)}_\phi$ where $K^{(1)}_\phi$ = 1(kJ·mol^{-1}).

The nonbonded part of the Hamiltonian (H_{NB}) is

$$H_{NB} = \sum_{i=1}^{N-4} \sum_{j=i+4}^{N} \left[\varepsilon_0\left(5\left(\frac{r^0_{ij}}{r_{ij}}\right)^{12} - 6\left(\frac{r^0_{ij}}{r_{ij}}\right)^{10}\right)\Delta_{ij} + \varepsilon_r\left(\frac{\sigma}{r_{ij}}\right)^{12}\left(1 - \Delta_{ij}\right)\right].$$

Here we consider that if the i and j residues are in contact at the native configuration, then Δ_{ij} = 1; otherwise, Δ_{ij} = 0 and nonnative pairs (Δ_{ij} = 0) feel repulsive potential. Here, $\varepsilon_0 = \varepsilon_r$ = 1(kJ·mol^{-1}).

SBM Simulations. Initial structures were relaxed under the SB Hamiltonian and the structures of different equilibrium ensembles were collected from Langevin dynamics at low friction limit to improve sampling. Simulations were performed at 300 K. The equation of motion for Langevin dynamics used for integration is

$$m\ddot{\vec{r}}_i = -\zeta\dot{\vec{r}}_i - \partial_{\vec{r}_i}H(\{\vec{r}_i\}) + \vec{\Gamma}_i(t),$$

where ζ is the friction coefficient, $-\partial_{\vec{r}_i}H(\{\vec{r}_i\})$ is the conformational force, and $\vec{\Gamma}_i(t)$ is random force which satisfies $\langle\vec{\Gamma}_i(t).\vec{\Gamma}_j(t')\rangle = \left(6\zeta K_B T/h\right)\delta_{ij}(t - t')$ where $\zeta = 0.05\tau_L^{-1}$ and $h = 0.0025\tau_L$ with $\tau_L = \left(m\sigma^2/\varepsilon_0\right)^{1/2}$ were used. This low friction value was chosen for the purpose of effective conformational space sampling.

All-Atom Explicit Solvent Simulations and Free Energy Calculations. For the all-atom explicit solvent simulations, we have considered the MT-bound monomeric crystal structure of kinesin (PDB ID code 4LNU) (26) in the presence and absence of propofol. We also included the possibility for the kinesin head (without MT) to be bound to either propofol or fropofol. We performed simulations using the GROMOCS96 53a6 force field (64) and the SPC water model using the GROMACS simulation package (65). The simulation box sizes were 11.6 × 12.0 × 16.5 nm^3 with 70,951 water molecules for the kinesin–MT complex and 7.31 × 6.20 × 8.21 nm^3 with 10,696 water molecules for the free kinesin head in solution. Before energy minimization, we neutralized both systems, the kinesin–MT complex and the free kinesin head, by adding 32 and 5 counterions, respectively. The steepest descent minimization method was used to perform energy minimization and 1-ns NVT simulations with position restrain were carried out restraining the initial positions of the protein atoms by a harmonic potential. Finally, a 100-ns NPT simulation was performed using a V-rescale temperature coupling at a constant temperature bath of 300 K and Parrinello–Rahman pressure coupling at a constant pressure bath of 1 atm. The SHAKE algorithm (66) was used to keep all bonds rigid. A PME cutoff scheme (67) was used for the nonbonded interactions.

For free-energy calculations, an umbrella sampling technique (56) was implemented in GROMACS. To evaluate the binding free energy of the kinesin head on the MT in the presence and absence of propofol, we choose

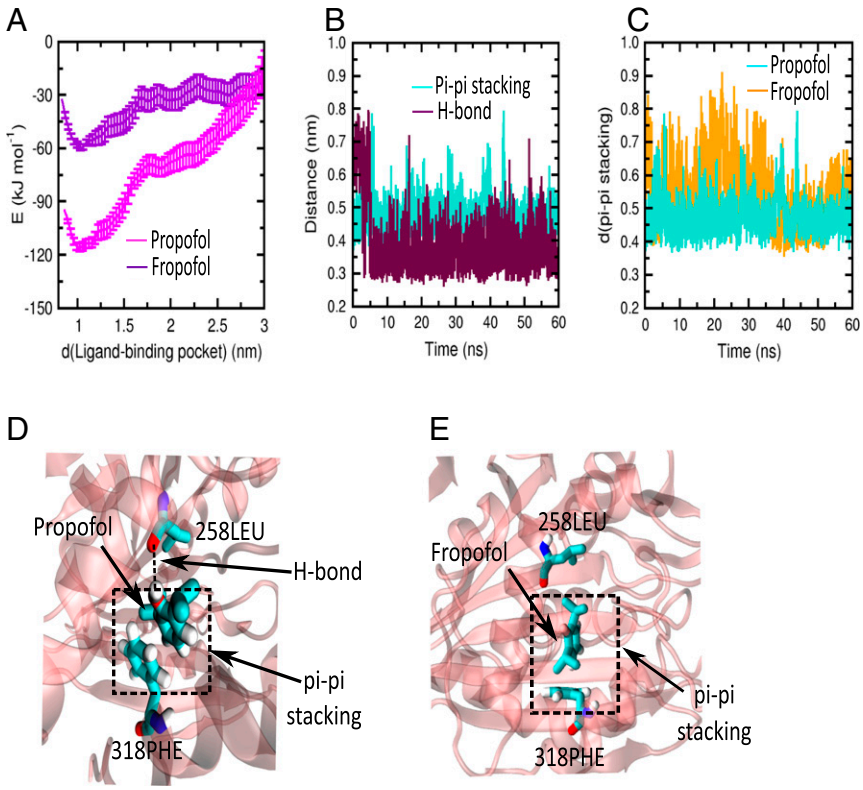

Fig. 9. Molecular picture of local interactions of propofol and fropofol in the kinesin-motor domain. (*A*) Binding free energy of propofol and fropofol at pocket-1 of the L head. Minima for fropofol is destabilized relative to propofol which indicates low binding affinity of fropofol. d(Ligand-binding pocket) indicates COM distance of ligand from the binding pocket where d represents distance. (*B*) Distances of pi–pi stacking interactions and H-bond interactions of 1-hydroxyl group of propofol with 318PHE and backbone -CO of 258LEU respectively. (*C*) For fropofol the pi–pi stacking interactions fluctuate more than those of propofol. (*D*) Representation of pi–pi stacking and H-bond interactions in propofol-bound kinesin head. (*E*) The orientation of fropofol and 318PHE has changed and the increment of distance makes pi–pi stacking interactions less favorable. An H-bond interaction is not possible here as fropofol lacks the 1-hydroxyl group.

the COM distance between the head and the MT as an order parameter. Additionally, to calculate the propofol and fropofol binding free energies in the binding pocket, we considered the free kinesin head bound to propofol/fropofol in explicit solvent. The distance between the ligand and the binding pocket was used as an order parameter in these calculations. In each window, a biased force of 1,000 kJ·mol^{-1}·nm^{-2} was applied to fix the desired value for this distance and a 10-ns NPT production run was performed at a constant temperature for the bath of 300 K and at a constant pressure bath of 1 atm. The weighted histogram analysis method (56) was employed to extract the energy profile from the histogram of distances obtained by combining all windows.

Data Availability. All study data are included in the article and/or *SI Appendix*.

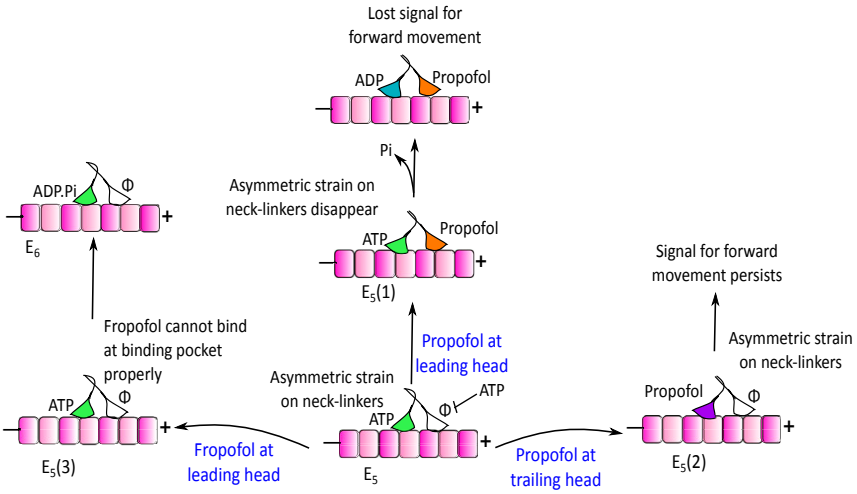

Fig. 10. A schematic diagram to show the effects of propofol and fropofol binding at the kinesin motor domain. The E_5 intermediate binds propofol at the leading head, which reduces the asymmetric strain between two NLs of the L and T heads (E_5 (1)). The loss in the asymmetric strain leads to the loss of the signal for the forward movement. Propofol at the trailing head is unable to reduce the asymmetric strain between the NLs [E_5 (2)] and kinesin moves forward [E_5 (3)]. Fropofol cannot bind at the pocket-1 properly and does not show any significant effect on kinesin motility.

ACKNOWLEDGMENTS. B.J. and M.D. were supported by the Department of Science and Technology (DST) Science and Engineering Research Board grant CRG/2020/000756. J.N.O. was supported by the Center for Theoretical Biological Physics sponsored by the NSF (Grant PHY-2019745), by the Welch Foundation (Grant C-1792), and by NSF-CHE-1614101. J.N.O. is a Cancer Prevention and Research Institute of Texas Scholar in Cancer Research. S.P.G. was supported by the NIH grant R37-GM054141. M.D. is supported by DST fellowship and Indian Association for the Cultivation of Science fellowship.

1. Y. Kotani, M. Shimazawa, S. Yoshimura, T. Iwama, H. Hara, The experimental and clinical pharmacology of propofol, an anesthetic agent with neuroprotective properties. *CNS Neurosci. Ther.* **14**, 95–106 (2008).
2. B. T. Bateman, A. S. Kesselheim, Propofol as a transformative drug in anesthesia: Insights from key early investigators. *Drug Discov. Today* **20**, 1012–1017 (2015).
3. P. Tang, R. Eckenhoff, Recent progress on the molecular pharmacology of propofol. *F1000 Res.* **7**, 123 (2018).
4. H. C. Hemmings Jr *et al*., Towards a comprehensive understanding of anesthetic mechanisms of action: A decade of discovery. *Trends Pharmacol. Sci.* **40**, 464–481 (2019).
5. M. D. Krasowski *et al*., General anesthetic potencies of a series of propofol analogs correlate with potency for potentiation of gamma-aminobutyric acid (GABA) current at the GABA(A) receptor but not with lipid solubility. *J. Pharmacol. Exp. Ther.* **297**, 338–351 (2001).
6. D. S. Stewart *et al*., p-(4-Azipentyl)propofol: A potent photoreactive general anesthetic derivative of propofol. *J. Med. Chem.* **54**, 8124–8135 (2011).
7. S. S. Jayakar *et al*., Multiple propofol-binding sites in a γ-aminobutyric acid type A receptor (GABAAR) identified using a photoreactive propofol analog. *J. Biol. Chem.* **289**, 27456–27468 (2014).
8. K. A. Woll *et al*., A novel bifunctional alkylphenol anesthetic allows characterization of γ-aminobutyric acid, type A (GABAA), receptor subunit binding selectivity in synaptosomes. *J. Biol. Chem.* **291**, 20473–20486 (2016).
9. T. Meng *et al*., Molecular mechanism of anesthetic-induced depression of myocardial contraction. *FASEB J.* **30**, 2915–2925 (2016).
10. D. C. Chiara *et al*., Photoaffinity labeling the propofol binding site in GLIC. *Biochemistry* **53**, 135–142 (2014).
11. M. B. Kelz, G. A. Mashour, The biology of general anesthesia from paramecium to primate. *Curr. Biol.* **29**, R1199–R1210 (2019).
12. B. M. Bensel *et al*., Common general anesthetic propofol impairs kinesin processivity. *Proc. Natl. Acad. Sci. U.S.A.* **114**, E4281–E4287 (2017).
13. N. Hirokawa, S. Niwa, Y. Tanaka, Molecular motors in neurons: Transport mechanisms and roles in brain function, development, and disease. *Neuron* **68**, 610–638 (2010).
14. K. J. Verhey, N. Kaul, V. Soppina, Kinesin assembly and movement in cells. *Annu. Rev. Biophys.* **40**, 267–288 (2011).
15. M. Bentley, G. Banker, The cellular mechanisms that maintain neuronal polarity. *Nat. Rev. Neurosci.* **17**, 611–622 (2016).
16. P. Guedes-Dias, E. L. F. Holzbaur, Axonal transport: Driving synaptic function. *Science* **366**, eaaw9997 (2019).
17. S. Rice *et al*., A structural change in the kinesin motor protein that drives motility. *Nature* **402**, 778–784 (1999).
18. Z. Zhang, D. Thirumalai, Dissecting the kinematics of the kinesin step. *Structure* **20**, 628–640 (2012).
19. Z. Zhang, Y. Goldtzvik, D. Thirumalai, Parsing the roles of neck-linker docking and tethered head diffusion in the stepping dynamics of kinesin. *Proc. Natl. Acad. Sci. U.S.A.* **114**, E9838–E9845 (2017).
20. C. L. Asbury, A. N. Fehr, S. M. Block, Kinesin moves by an asymmetric hand-over-hand mechanism. *Science* **302**, 2130–2134 (2003).
21. A. Yildiz, M. Tomishige, R. D. Vale, P. R. Selvin, Kinesin walks hand-over-hand. *Science* **303**, 676–678 (2004).
22. R. Takaki, M. L. Mugnai, Y. Goldtzvik, D. Thirumalai, How kinesin waits for ATP affects the nucleotide and load dependence of the stepping kinetics. *Proc. Natl. Acad. Sci. U.S.A.* **116**, 23091–23099 (2019).
23. K. Kaseda, H. Higuchi, K. Hirose, Alternate fast and slow stepping of a heterodimeric kinesin molecule. *Nat. Cell Biol.* **5**, 1079–1082 (2003).
24. K. A. Woll *et al*., Role for the propofol hydroxyl in anesthetic protein target molecular recognition. *ACS Chem. Neurosci.* **6**, 927–935 (2015).
25. K. A. Woll *et al*., An allosteric propofol-binding site in kinesin disrupts kinesin-mediated processive movement on microtubules. *J. Biol. Chem.* **293**, 11283–11295 (2018).
26. L. Cao *et al*., The structure of apo-kinesin bound to tubulin links the nucleotide cycle to movement. *Nat. Commun.* **5**, 5364 (2014).
27. B. Gigant *et al*., Structure of a kinesin-tubulin complex and implications for kinesin motility. *Nat. Struct. Mol. Biol.* **20**, 1001–1007 (2013).
28. M. L. Mugnai, C. Hyeon, M. Hinczewski, D. Thirumalai, Theoretical perspective on biological machines. *Rev. Mod. Phys.* **92**, 025001 (2020).
29. B. E. Clancy, W. M. Behnke-Parks, J. O. L. Andreasson, S. S. Rosenfeld, S. M. Block, A universal pathway for kinesin stepping. *Nat. Struct. Mol. Biol.* **18**, 1020–1027 (2011).
30. Q. Shao, Y. Q. Gao, On the hand-over-hand mechanism of kinesin. *Proc. Natl. Acad. Sci. U.S.A.* **103**, 8072–8077 (2006).
31. A. Yildiz, M. Tomishige, A. Gennerich, R. D. Vale, Intramolecular strain coordinates kinesin stepping behavior along microtubules. *Cell* **134**, 1030–1041 (2008).
32. J. O. Andreasson *et al*., Examining kinesin processivity within a general gating framework. *eLife* **4**, e07403 (2015).
33. X. X. Shi, S. K. Guo, P. Y. Wang, H. Chen, P. Xie, All-atom molecular dynamics simulations reveal how kinesin transits from one-head-bound to two-heads-bound state. *Proteins* **88**, 545–557 (2020).
34. C. Hyeon, J. N. Onuchic, Internal strain regulates the nucleotide binding site of the kinesin leading head. *Proc. Natl. Acad. Sci. U.S.A.* **104**, 2175–2180 (2007).
35. A. Czövek, G. J. Szöllosi, I. Derényi, Neck-linker docking coordinates the kinetics of kinesin's heads. *Biophys. J.* **100**, 1729–1736 (2011).
36. V. Hariharan, W. O. Hancock, Insights into the mechanical properties of the kinesin neck linker domain from sequence analysis and molecular dynamics simulations. *Cell. Mol. Bioeng.* **2**, 177–189 (2009).
37. M. Lo Giudice *et al*., A missense mutation in the coiled-coil domain of the KIF5A gene and late-onset hereditary spastic paraplegia. *Arch. Neurol.* **63**, 284–287 (2006).
38. M. Dutta, M. R. Diehl, J. N. Onuchic, B. Jana, Structural consequences of hereditary spastic paraplegia disease-related mutations in kinesin. *Proc. Natl. Acad. Sci. U.S.A.* **115**, E10822–E10829 (2018).
39. M. Dutta, B. Jana, Exploring the mechanochemical cycle of dynein motor proteins: Structural evidence of crucial intermediates. *Phys. Chem. Chem. Phys.* **18**, 33085–33093 (2016).
40. M. Dutta, B. Jana, Role of AAA3 domain in allosteric communication of dynein motor proteins. *ACS Omega* **4**, 21921–21930 (2019).
41. R. N. Manna, M. Dutta, B. Jana, Mechanistic study of the ATP hydrolysis reaction in dynein motor protein. *Phys. Chem. Chem. Phys.* **22**, 1534–1542 (2020).
42. B. Jana, C. Hyeon, J. N. Onuchic, The origin of minus-end directionality and mechanochemistry of Ncd motors. *PLoS Comput. Biol.* **8**, e1002783 (2012).
43. B. Jana, J. N. Onuchic, Strain mediated adaptation is key for myosin mechanochemistry: Discovering general rules for motor activity. *PLoS Comput. Biol.* **12**, e1005035 (2016).
44. Q. Wang *et al*., Molecular origin of the weak susceptibility of kinesin velocity to loads and its relation to the collective behavior of kinesins. *Proc. Natl. Acad. Sci. U.S.A.* **114**, E8611–E8617 (2017).
45. Q. Wang *et al*., Molecular mechanisms of the interhead coordination by interhead tension in cytoplasmic dyneins. *Proc. Natl. Acad. Sci. U.S.A.* **115**, 10052–10057 (2018).
46. R. Kanada, T. Kuwata, H. Kenzaki, S. Takada, Structure-based molecular simulations reveal the enhancement of biased Brownian motions in single-headed kinesin. *PLoS Comput. Biol.* **9**, e1002907 (2013).
47. S. Kubo, W. Li, S. Takada, Allosteric conformational change cascade in cytoplasmic dynein revealed by structure-based molecular simulations. *PLoS Comput. Biol.* **13**, e1005748 (2017).
48. Y. Goldtzvik, Z. Zhang, D. Thirumalai, Importance of hydrodynamic interactions in the stepping kinetics of kinesin. *J. Phys. Chem. B* **120**, 2071–2075 (2016).
49. M. Dutta, B. Jana, Computational modeling of dynein motor proteins at work. *Chem. Commun. (Camb.)*, 10.1039/D0CC05857B (2020).
50. O. Trott, A. J. Olson, AutoDock Vina: Improving the speed and accuracy of docking with a new scoring function, efficient optimization, and multithreading. *J. Comput. Chem.* **31**, 455–461 (2010).
51. J. K. Noel *et al*., SMOG 2: A versatile software package for generating structure-based models. *PLoS Comput. Biol.* **12**, e1004794 (2016).
52. J. K. Noel, P. C. Whitford, K. Y. Sanbonmatsu, J. N. Onuchic, SMOG@ctbp: Simplified deployment of structure-based models in GROMACS. *Nucleic Acids Res.* **38**, W657–W661 (2010).
53. K. Okazaki, N. Koga, S. Takada, J. N. Onuchic, P. G. Wolynes, Multiple-basin energy landscapes for large-amplitude conformational motions of proteins: Structure-based molecular dynamics simulations. *Proc. Natl. Acad. Sci. U.S.A.* **103**, 11844–11849 (2006).
54. J. N. Onuchic, P. G. Wolynes, Theory of protein folding. *Curr. Opin. Struct. Biol.* **14**, 70–75 (2004).
55. F. Kozielski *et al*., The crystal structure of dimeric kinesin and implications for microtubule-dependent motility. *Cell* **91**, 985–994 (1997).
56. S. Kumar, J. M. Rosenberg, D. Bouzida, R. H. Swendsen, P. A. Kollman, THE weighted histogram analysis method for free-energy calculations on biomolecules. I. The method. *J. Comput. Chem.* **13**, 1011–1021 (1992).
57. L. Qiu *et al*., The role of the hydroxyl group in propofol-protein target recognition: Insights from ONIOM studies. *J. Phys. Chem. B* **121**, 5883–5896 (2017).
58. G. M. Morris *et al*., AutoDock4 and AutoDockTools4: Automated docking with selective receptor flexibility. *J. Comput. Chem.* **30**, 2785–2791 (2009).
59. D. Baker, A surprising simplicity to protein folding. *Nature* **405**, 39–42 (2000).
60. P. E. Leopold, M. Montal, J. N. Onuchic, Protein folding funnels: A kinetic approach to the sequence-structure relationship. *Proc. Natl. Acad. Sci. U.S.A.* **89**, 8721–8725 (1992).
61. D. Thirumalai, Z. Liu, E. P. O'Brien, G. Reddy, Protein folding: From theory to practice. *Curr. Opin. Struct. Biol.* **23**, 22–29 (2013).
62. H. Lammert, A. Schug, J. N. Onuchic, Robustness and generalization of structure-based models for protein folding and function. *Proteins* **77**, 881–891 (2009).
63. S. Takada, Gō model revisited. *Biophys. Physicobiol.* **16**, 248–255 (2019).
64. C. Oostenbrink, A. Villa, A. E. Mark, W. F. van Gunsteren, A biomolecular force field based on the free enthalpy of hydration and solvation: The GROMOS force-field parameter sets 53A5 and 53A6. *J. Comput. Chem.* **25**, 1656–1676 (2004).
65. M. J. Abraham *et al*., GROMACS: High performance molecular simulations through multi-level parallelism from laptops to supercomputers. *SoftwareX* **1-2**, 19–25 (2015).
66. V. Kräutler, W. F. van Gunsteren, P. H. Hünenberger, A fast SHAKE algorithm to solve distance constraint equations for small molecules in molecular dynamics simulations. *J. Comput. Chem.* **22**, 501–508 (2001).
67. S. Páll, B. Hess, A flexible algorithm for calculating pair interactions on SIMD architectures. *Comput. Phys. Commun.* **184**, 2641–2650 (2013).